BERGY-BIT MOTION DUE TO WIND, WAVE, CURRENT AND CORIOLIS FORCES

R. Doyle[+] and M. Arockiasamy[++]

Faculty of Engineering,
Memorial University,
St. John's, Newfoundland, Canada
([+]Undergraduate Student [++]Associate Professor)

ABSTRACT

Bergy-bits and growlers pose a threat to offshore structures, such as semi-submersibles and drillships, drilling off the Avalon coasts of Newfoundland and Labrador. The paper presents a study for predicting the motions of a bergy-bit under a variety of wind, wave and current conditions. The forces acting on the bergy-bit were modelled by a Morison type equation which included wind, wave and wind/wave generated current components. The non-linearity associated with the viscous fluid drag, and available inertial and drag coefficients, were considered in determining the excitation forces. A computer code was developed to obtain the displacements, velocities and accelerations of the bergy-bit masses for selected wave conditions with different amplitudes, periods and inertial and drag coefficients. The drifting motions of the bergy-bit under a given wind/wave excitation and Coriolis forces were also examined considering the inertial and drag forces.

INTRODUCTION

Renewed interest in the factors which influence iceberg and bergy-bit motion has been generated by recent offshore exploration activity and the desire to better understand iceberg drift and oscillatory motion under wind, current and wave forces.

In order to predict bergy-bit motion, it is first necessary to determine the excitation forces that act on it. The most obvious of these are the inertial and drag forces exerted by fluid particle motion over the bergy-bit. Other forces include Coriolis forces, sea surface slope (pressure gradient) forces, gravity forces, and forces generated through swells.

In this study, an effort is made to integrate the oscillation and motion of bergybits due to wind/wave currents and wave particle motion over the body causing oscillatory "drag" and "inertial" forces. In addition, the influence of the earth's rotation on the motion of bergybits is considered in the form of "Coriolis" components.

LITERATURE REVIEW

The major factor affecting the design of offshore structures that are or would be located off the Eastern Coasts of Newfoundland and Labrador, is the complex ice regime comprised of icebergs/bergy-bits and a seasonal ice cover or pack-ice conditions.

The majority of icebergs that drift along the "Iceberg Alley" off the coasts of Newfoundland and Labrador are calved from the glaciers of West Greenland with smaller populations originating from East Greenland and the Canadian Archipelago [Napoleoni (1979), Wright and Berenger (1980)]. These icebergs (from which bergy-bits are calved) drift southward along the coasts of Labrador and Newfoundland; they are subjected to entrapment in bays, isolated fjords or Arctic pack ice, grounding in bathymetric rise or shallow regions [Grande and Guilleaud (1984)], or deterioration due to the sea ice

Proceedings, Eastern Snow Conference, V. 29, 41st Annual Meeting, Washington, D.C., June 7-8, 1984

conditions and sea surface temperatures as they move south. The annual variation in iceberg population south of 48°N latitude from 1935 to 1978 is shown in Fig. 1.1 [Petroleum Directorate (1981)]. Of the 10,000 to 15,000 icebergs which are calved annually from the West Greenland glaciers, an average of 380 cross the 48th parallel [Murray (1969)]. As Fig. 1 shows, the number of bergs that cross the 48° parallel vary from year to year, being almost zero during some years and a maximum of about 1,600 in 1972.

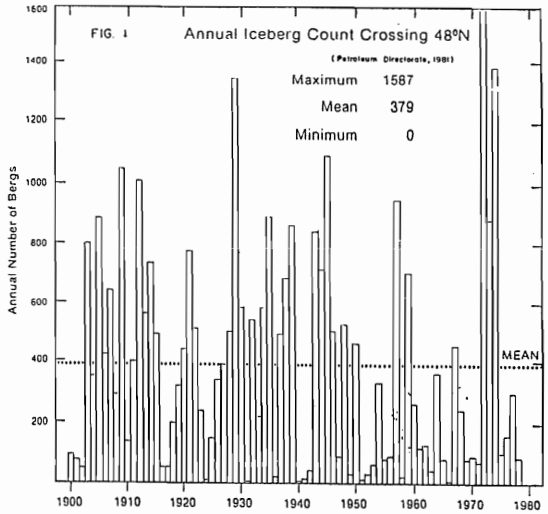

Icebergs vary greatly in shape, and classification is extremely difficult. Simplified classification schemes typically contain no less than eight iceberg types such as block, drydock, dome, pinnacled, tabular, crescent, pinnacled crescent and tilted tabular [NORDCO (1975)]. Since the main drift of the Labrador Current is from the northwest to the southeast, this is also the predominant direction for iceberg movement. However, since current and wind patterns are both highly variable on a short time scale, iceberg drift also shows short time scale variability [Dempster (1974)]. Iceberg drift speed varies with mass, with the larger bergs moving at lower velocities than smaller ones. A summary of the mean and maximum iceberg speeds for five sites monitored during 1973, '74 and '75 Labrador offshore drilling seasons are shown in Table I [Wright and Berenger (1980)]. The average velocities range from 0.1 to 0.3 m/s while the maximum velocities range from 0.5 to 1.2 m/s.

TABLE 1 ICEBERG SPEEDS [Wright and Berenger (1980)]

Drilling Site and Latitude	Time	Average (and Maximum) speeds (m/sec)
Freydis 53° 5'N	July 4-Aug. 8 (1973)	0.15 (0.66)
Leif 54° 17'N	July 28-Sept. 4 (1973)	0.19 (0.53)
Gudrid 54° 54'N	July 10-Oct. 2 (1974)	0.19 (1.23)
Shorri 57° 20'N	Aug. 25-Oct. 8 (1975)	0.17 (0.73)
Karlsefni 58° 52'N	Aug. 10-Sept. 25 (1975)	0.27 (0.94)

Napoleoni (1979) considered wind forces, wind/wave generated current drag forces, Coriolis forces due to the earth's rotation, pressure forces, and towing forces while computing the drift motion of an iceberg. Using a constant geostrophic current and a

time-dependent Ekman current, Mountain (1980) proposed a mathematical model to predict the drift of an iceberg and checked the model against observed drifts of icebergs. Taking into account the environmental forces due to water drag, wind drag, Coriolis acceleration and sea surface slope, Sodhi and El-Tahan (1980) developed a numerical model for iceberg drift trajectories. The comparison between observed and predicted iceberg drift was found to be good. From the analysis of available studies on maximum drift velocity of hundreds of icebergs tracked at 15 drilling sites offshore Labrador, El-Tahan, El-Tahan and Venkatesh (1983) indicated that only 20% of the 260 tracked icebergs had maximum speeds in excess of 0.75 m/sec, and only 7% of the tracked icebergs had a maximum velocity of 1.0 m/sec or more. The probability of an iceberg to drift with a maximum speed in excess of 1.2 m/sec was estimated to be less than 1%. The periods of "heaving" (or "bobbing") and "rocking" oscillations of the massive Antarctic icebergs were computed by Schwedtfeger (1980) and found to vary between 1 to 30 secs. Foldvik, Gammelsrod and Gjessing (1980) measured the oscillation periods of Antarctic icebergs to vary between 16 to 50 secs. Flexural response of a tabular ice island was measured experimentally in Kong Oscars Fjord, East Greenland, in September 1978 by Goodman, Wadhams and Squire (1980). Hsiung and Aboul-Azm (1983) determined the motion response of a 200,000 t tabular iceberg to wave-force excitations, considering first order and second order wave forces acting on the iceberg. They stated that the effect of waves must also be considered in predicting correctly the drift path of the icebergs. Lever, Reimer and Diemand (1984) and Murray, Muggeridge and Guy (1983) carried out tank tests on moving ice masses under regular and grouped waves. Lever, Reimer and Diemand (1984) stated that the ice masses which are smaller than 1/13 the wave length moved like wave particles. Till date, no analytical study has been made on the detailed wave oscillation of a moving ice mass under current and wave excitation. Since the wave and wind currents are likely to co-exist along with the wave excitation, the analytical model also considers the effect of the presence of currents on the motion of ice masses; in addition, the influence of Coriolis forces are also considered in the analytical model. The present study was prompted by an earlier study carried out by Loo (1983) on wave forces and semi-submersible bergy-bit collision.

The presence of a wind/wave generated steady current changes the wave particle velocities experienced over its "body" by a floating structure. Using Morison-O'Brien's (1950) approach, the forces acting on the body are computed using the fluid particle velocities and accelerations. The "relative velocity and acceleration" concept is used while computing the "drag" and "inertial" forces acting on the floating body.

EXCITATION FORCES ACTING ON THE BERGY-BIT

Wave Characteristics

For the purpose of this numerical model, the horizontal water-particle velocities and accelerations given by the linear Airy's wave theory were considered. There are two different formulations for determining water-particle velocities and accelerations. The formulation used to model the water particle velocity and accelerations corresponds to deep water conditions. This alternative was chosen to minimize the detailed numerical computations involved in the integration over the submerged portion of the bergy-bit. According to an earlier study [Loo (1983)], the $\frac{d}{L}$ ratios varied between 0.52 (H=10.0 m; T = 11.0 secs) and 0.331 (H=20.0 m, T=13.8 secs); hence the error introduced in wave particle velocities due to this simplification is considered to be around 5% to 10%.

In 'deepwater', $\frac{d}{L} \geq 0.5$, where d = water depth, L = wave length.

$$U = \frac{\pi H}{T} e^{\left(\frac{2\pi y}{L_0}\right)} \cos 2\pi \left(\frac{x}{L} - \frac{t}{T}\right)$$

$$\dot{U} = \frac{2\pi^2 H}{T^2} e^{\frac{2\pi y}{L_0}} \sin 2\pi \left(\frac{x}{L} - \frac{t}{T}\right) \qquad (1)$$

where x is the distance along the wave direction, y, the vertical distance measured from the free-water surface, and L_0 the deep-water wave-length.

When solving for the wavelength of the selected wave, the third order Stoke's wave theory was chosen [Loo (1983)]. The following equation expresses wavelength, L, as a function of wave height, H, wave period, T, and water depth, d.

$$L = \frac{gT^2}{2\pi} \tanh\left(\frac{2\pi d}{L}\right)\left[1+\left(\frac{2\pi a}{L}\right)^2\left(\frac{14 + 4\cosh(4\pi\, d/L)}{16\sinh(2\pi\, d/L)}\right)\right] \tag{2}$$

where a is a parameter obtained from the solution of an auxiliary cubic algebraic equation.

Since only a single-degree-of-freedom model is used to investigate the motion of the bergy-bit, the fluid velocity U and acceleration $\dot{U}$ are expressed as the velocity U_G and acceleration $\dot{U}_G$ averaged over the submerged height and length of the bergy-bit, and acting at the centroid of the bergy-bit. Consider first the fluid velocity. The average fluid velocity U_G is obtained as,

$$U_G = \frac{HL_0L}{4\pi\, hL_b T\pi}\left(1-e^{-\frac{2\pi h}{L_0}}\right)\left\{\sin\left[\frac{2\pi(\eta + L_b)}{L} - \omega t\right] - \sin\left[\frac{2\pi\eta}{L} - \omega t\right]\right\} \tag{3}$$

where

η = displacement along wave direction
L_b = length of body

$L_0 = 1.56\ T^2$, deep-water wave length

ω = freq = $2\pi/T$

The average fluid acceleration is obtained as

$$\dot{U}_G = -\frac{2\pi}{T}\left(\frac{HL_0L}{4\pi hL_bT}\right)\left(1 - e^{-\frac{2\pi h}{L_0}}\right)\left\{\cos\left[\frac{2\pi(\eta+L_b)}{L} - \omega t\right] - \cos\left(\frac{2\pi\eta}{L} - \omega t\right)\right\} \tag{4}$$

Characteristics of Wind/Wave Current

The introduction of current components directly influences the fluid particle velocities and drag forces. Without current, all body displacements occur along the direction of wave particle motion. The introduction of a variable wind current angle allows displacements which, when resolved, will have components along two perpendicular directions. For these conditions the waves are assumed to be fetch-controlled; in other words, the wind has been uninterrupted over a sufficiently long distance that the waves on the ocean's surface travel in the same direction as the wind. The same assumption is made for the wave induced current.

Wave Induced Current

The wave induced current derivation is based upon the finite height Stokian wave theory which assumes a non-zero mass transport velocity. The wave-induced mean drift velocity at the sea surface is in general [Memos (1979)],

$$U_{c_{w_1}} = w[A(f,j)]^2\ [S(f,j)]^3\ H(kd) \tag{5}$$

where

$$A(f,j) = \frac{ga}{w^2}\ ,\quad S(f,j) = \frac{w\ \sigma}{g},\quad f = (gF)^{1/2}\ ,\quad j = \frac{(gd)^{1/2}}{w} \tag{6}$$

with w = being the wind speed, F, the fetch length, g, acceleration due to gravity, a, amplitude of the significant waves and σ, frequency of the significant waves. For shallow water

$$H(kd) = \frac{\cosh kd}{4 \sinh^3 kd} \{2 \cosh 2kd + \frac{\sinh 2kd}{2kd} [2(kd)^2 - 3] - \frac{3}{2} \} \quad (7)$$

For deep water,

$$H(kd) = 1 - \frac{1}{2kd} \quad (8)$$

For deep water ($kd \gg 1$) conditions, $A(f,j)$ and $S(f,j)$ are functions of the fetch only. As previously mentioned, the numerical model will consider only deep water conditions, and hence only Eqn. (8) is utilised.

Wind Induced Current

In the previous formulation, the current was generated by the wind through the generation of waves. This section deals with the current directly generated by the drag force of the wind acting over a frictional layer extending below the water surface.

The pure wind drift current (or the Ekman current, has been developed on the assumption that, apart from the driving force, the only forces present are the Coriolis force and the friction between successive horizontal layers. For deep water, the wind induced current velocity at the surface is [Memos (1979)],

$$U_{c_{w_2}} = \frac{\pi\tau}{\sqrt{2}\, DP\Omega \sin\psi} \quad (9)$$

where

$$D = \pi \sqrt{\frac{\mu_e}{\rho\Omega \sin\psi}}, \quad \tau = \rho' \, c(w) \, w^2 \quad (10)$$

with τ being shear stress, D thickness of frictional layer, Ω = rotational speed of earth, ψ = latitude (rad), μ_e = eddy viscosity of water, ρ' = air density, and w = wind speed. Also

$$\begin{aligned} c(w) &= (7 + 1.2\, w)\, 10^{-4} && w < 14 \text{ m/sec} \\ c(w) &= 2.4 \times 10^{-3} && w > 14 \text{ m/sec} \end{aligned} \quad (11)$$

The depth of the frictional layer is defined by the depth where the current direction is opposite to the surface current direction. The angle between the direction of the wind and the surface current is given by [Fig. 2]

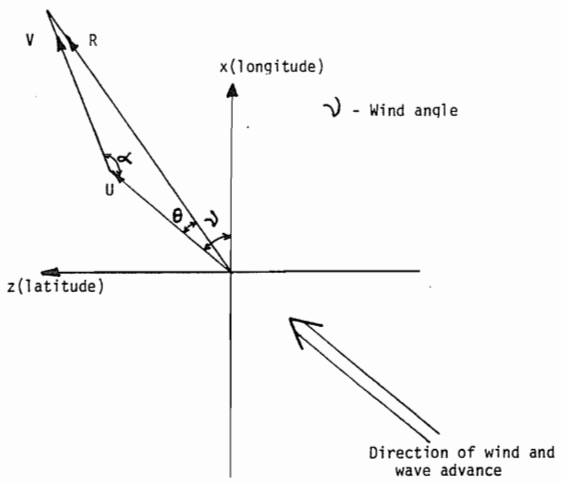

RESULTANT OF WAVE- AND WIND- CURRENT VELOCITIES

Fig. 2

$$\alpha = \tan^{-1} \frac{\text{Sinh } h_1 - \text{Sin } h_1}{\text{Sinh } h_1 + \text{Sin } h_1} \tag{12}$$

where

$$h_1 = \frac{2\pi d}{D} \tag{13}$$

If U represents wave current velocity and V represents wind current velocity a resultant R can be found by:

$$R^2 = U^2 + V^2 - 2UV \cos \alpha \tag{14}$$

The angle between the direction of the current resultant and the wave direction is

$$\theta = \sin^{-1} \left(\frac{V \sin \alpha}{R}\right) \tag{15}$$

It should be noted that since the wave generated current is in the direction of wave advance, the pure wind induced current is responsible for the angle (θ) between the current resultant and the wind/wave direction. This angle will be to the right of wind advance in the northern hemisphere and to the left in the southern. The wind and wave generated current components can be added vectorially to the fluid velocities. The final direction of the bergy-bit motion will be dependent upon the given wind direction. It is therefore adventageous to resolve the fluid and body velocities into orthogonal components, one corresponding to the latitude direction and the other the longitude. Overall fluid velocities can now be written as

$$\bar{U} = \bar{U}_{c_{w_1}} + \bar{U}_{c_{w_2}} + \bar{U}_w \tag{16}$$

where $\bar{U}_w$ is the wave particle velocity.

Review of Water-Particle Velocities and Accelerations for Wave Current

If we consider the latitude direction the z-direction and the longitude the x-direction, the average fluid particle velocity components due to wave and current are given by,

$$U_{x_G} = \frac{HL_0 L \cos \nu}{4hL_b T\pi}\left(1-e^{-\frac{2\pi H}{L_0}}\right)\left\{\sin\left[2\pi\left(\frac{\eta+L_b}{L}\right)-\omega t\right]-\sin\left(\frac{2\pi\eta}{L} - \omega t\right)\right\} + U_{c_x}$$

$$U_{z_G} = \frac{HL_0 L \sin \nu}{4hL_b T\pi}\left(1-e^{-\frac{2\pi h}{L_0}}\right)\left\{\sin\left[2\pi\frac{(\eta+L_b)}{L} - \omega t\right]- \sin\left(\frac{2\pi\eta}{L} - \omega t\right)\right\}+U_{c_z} \tag{17}$$

Since the current components are not time dependent, the fluid-particle accelerations can be written as

$$\dot{U}_{x_G} = -\frac{HL_0 L \cos \nu}{2h\, L_b\, T^2}\left(1-e^{-\frac{2\pi h}{L_0}}\right)\left\{\cos\left[2\pi\left(\frac{\eta+L_b}{L}\right)-\omega t\right]-\cos\left(\frac{2\pi\eta}{L} - \omega t\right)\right\}$$

$$\dot{U}_{z_G} = -\frac{HL_0 L \sin \nu}{2h\, L_b T^2}\left(1-e^{-\frac{2\pi h}{L_0}}\right)\left\{\cos\left[2\pi\left(\frac{\eta+L_b}{L}\right)-\omega t\right] - \cos\left(\frac{2\pi\eta}{L} - \omega t\right)\right\} \tag{18}$$

It should be noted that the term η represents the displacement along the wave direction. This displacement is common to both the longitude and latitude fluid velocity computations.

Wave Forces

Under wave force excitation, the Morison Equation [Morison et al, (1950)] can be expressed as

$$dF = dF_d + dF_I = \frac{1}{2} C_d \rho B |U-\dot{X}| (U-\dot{X}) dy + C_m \rho A (\dot{U}-\ddot{X}) dy \tag{19}$$

where

$$F = \int_{\eta}^{\eta+L_b} \int_{-h}^{0} dF \, dx \tag{20}$$

with dy being an incremental length over the body height, F_d drag force acting on the bergy-bit, F_I inertial force acting on the bergy bit, F total force in the direction of wave particle velocity and acceleration, and $\ddot{X}$, $\dot{X}$ acceleration and velocity of the bergy-bit, respectively.

In the analytical model, the freewater surface was set equal to the mean water elevation since it was found from an earlier study [Loo(1983)] that the computation of forces erred only by about 10% to 15% for slender towers. Therefore the water drag force is approximated as:

$$F_d = \int_{\eta}^{\eta+L_b} [\int_{-h}^{0} \frac{1}{2} C_d \rho B |U - \dot{X}| (U - \dot{X}) dy] dx \tag{21}$$

Using Eqn. 3, and assuming that the forces are acting at the center of gravity of the bergy-bit, the terms of integration can be assumed as the square of the averaged out relative velocity of the body. Hence the fluid drag force can be expressed by,

$$F_d = \frac{1}{2} C_d \rho B h \, \text{Sign} \left[\frac{HL_0L}{4\pi h L_b T} (1-e^{-\frac{2\pi h}{L_0}}) \{\sin[2\pi(\frac{\eta+L_b}{L}) - \omega t] - \sin(\frac{2\pi\eta}{L} - \omega t)\} - \dot{X}\right]^2 \tag{22}$$

where sign denotes the algebraic sign (+1 or -1) indicating the difference between the fluid and body velocities. The remaining force to be considered, in this simplified analysis, is the inertial force which can be expressed by,

$$F_I = C_m \rho A.h.\{-\frac{HL_0L}{2 h L_b T^2} (1 - e^{-\frac{2\pi h}{L_0}}) \{\cos [2\pi (\frac{\eta + L_b}{L}) - \omega t] - \cos (\frac{2\pi\eta}{L} - \omega t)\} - \ddot{X}] \tag{23}$$

Coriolis Force Components

The Coriolis force acting on the bergy-bit, is dependent upon the rotational speed of the earth and the location of the body on the earth's surface. The effect of earth's rotation was considered previously in the development of the Ekman pure wind drift current (Art 3.2.3). The following section will determine the Coriolis force components which will add to the forces acting on the bergy-bit as a result of its body velocity. Generally, the Coriolis force is given by

$$f_c = 2M_i \bar{\Omega} \times \bar{V}_i \tag{24}$$

with M_i being mass of bergy-bit, $\bar{\Omega}$, Earth's rotational vector and $\bar{V}_i$, the body velocity vector.

The position of the bergy-bit on the earth's surface can be specified by the latitude (denoted by ψ) and by angle ϕ, the bergy-bit motion makes with respect to the

latitude axis (Fig.3).

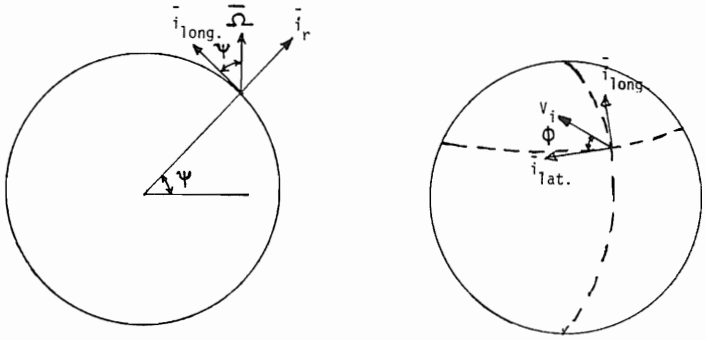

VECTOR DIRECTIONS FOR CORIOLIS FORCE COMPONENTS

Fig. 3

Earth's rotation ($\bar{\Omega}$) and the bergy-bit velocity (V_i) are given by,

$$\bar{\Omega} = \Omega (\cos \psi \, \bar{i}_{long} + \sin \psi \, \bar{i}_r)$$

$$\bar{V}_i = V_i (\text{Cos } \phi \, \bar{i}_{lat} + \sin \phi \, \bar{i}_{long}) \tag{25}$$

The terms $\bar{i}_{long}$, $\bar{i}_{lat}$, $\bar{i}_r$ represent orthogonal unit vectors along the longitude, latitude and radial directions. The Coriolis force can now be written as:

$$f_c = 2M_i \, V_i \, \Omega(-\sin \psi \sin \phi \, \bar{i}_{lat} + \sin \psi \cos \phi \, i_{long} - \cos \psi \cos \phi \, i_r) \tag{26}$$

Once again denoting the bergy-bit motion in latitude direction by Z and longitude by X, the following relationships can be obtained.

$$\dot{X} = V_i \sin \phi \qquad \dot{Z} = V_i \cos \phi \tag{27}$$

Therefore, the Coriolis force components in x and y directions are given by,

$$f_{c_x} = + 2M_i \, \Omega \sin \psi \; \dot{Z} \; , \; f_{c_z} = -2M_i \, \Omega \sin \psi \; . \; \dot{X} \tag{28}$$

EQUATIONS OF MOTION AND SOLUTION

Introduction

If we consider the bergy-bit as a single degree-of-freedom model of mass M_1 having a damping force C_1 and with no restoring forces as shown below (Fig. 4),

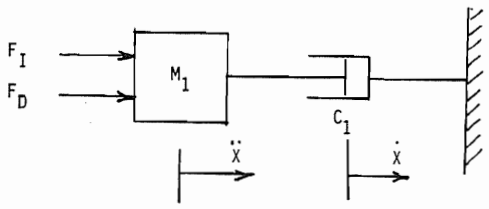

Fig. 4

The equation of motion can be expressed as

$$M_1 \ddot{X} + C_1 \dot{X} = F_I + F_d \tag{29}$$

Viscous Damping Coefficient

A special procedure given by Hooft (1982) is used to compute the frequency-dependent viscous damping coefficient. It involves the integration of the square of the forcing function divided by the wave amplitude, ie.,

$$C_1(\omega) = C_f \int_0^{2\pi} \{\frac{F(\mu,\omega)}{H/2}\}^2 \, d\mu \tag{30}$$

where

$$C_f = \frac{\omega^3 \cosh^2 kh}{4\pi \rho g^3 kh \tanh kh \, [1 + (\frac{\sin 2kh}{2kh})]} \tag{31}$$

and μ represents the one wave cycle in the direction of wave propagation. In the computer solution, this integration is approximated by Simpson's formula.

Total Force Components

The final equations of motion, which includes wind, wave, wind/wave currents and Coriolis effects, can now be written as:

Longitude direction - Positive towards north

$$\{M_1 + C_m \rho A h\} \ddot{X} + C_{1_x} \dot{X} = \tfrac{1}{2} C_d \rho B h \, sign_w \{[\frac{HL_0 L \cos \nu}{4h L_b T \pi}$$

$$(1-e^{-\frac{2\pi h}{L_0}}) \{\sin[2\pi(\frac{\eta+L_b}{L}) - \omega t] - \sin(\frac{2\pi\eta}{L} - \omega t)\} + U_{c_x}] - \dot{X}\}^2$$

$$+ \tfrac{1}{2} C_{d_{air}} \rho' B (h_T - h) \, Sign_a (w\cos\nu - \dot{X})^2 + 2 M_1 \Omega \sin\psi \, \dot{Z}$$

$$+ C_m \rho A h \{- \frac{HL_0 L \cos\nu}{2hL_b T^2} (1-e^{-\frac{2\pi h}{L_0}}) [\cos\{2\pi(\frac{\eta+L_b}{L}) - \omega t\} - \cos(\frac{2\pi\eta}{L} - \omega t)]\} \tag{32}$$

Similarly for the latitude direction - positive towards the west

$$\{M_1 + C_m \rho A.h\} \ddot{Z} + C_{1_z} \dot{Z} = \tfrac{1}{2} C_d \rho L_B h \, Sign_w \{[\frac{HL_0 L \sin \nu}{4h L_b T \pi}$$

$$(1-e^{-\frac{2\pi h}{L_0}}) \{\sin[2\pi(\frac{\eta+L_b}{L}) - \omega t] - \sin(\frac{2\pi\eta}{L} - \omega t)\} + U_{c_z}] - \dot{Z}\}^2$$

$$+ \tfrac{1}{2} C_{d_{air}} \rho' B (h_T - h) \, Sign_a (w \sin\nu - \dot{Z})^2 - 2 M_1 \Omega \sin\psi \, \dot{X}$$

$$+ C_m \rho .A .h \{- \frac{HL_0 L \sin\nu}{2hL_b T^2} (1-e^{-\frac{2\pi h}{L_0}}) [\cos\{2\pi(\frac{\eta+L_b}{L}) - \omega t\} - \cos(\frac{2\pi\eta}{L} - \omega t)]\} \tag{33}$$

The numerical solution of the equation of motion is obtained by the average acceleration method [Craig, (1981)]. The equaitons of motion developed in the numerical model are non-linear due to the square of the body velocity in the drag force terms. The solution of the motion equation is further complicated by the Coriolis force components whose direction is perpendicular to the related velocity components. The problems is overcome by a simultaneous solution of the latitude and longitude equations with a utilization of previously calculated variables to the forcing function. A major obstacle in the solution of the motion equations was the difficulty in determing the sign change in the forcing function. This problem arose because the forcing function was dependent upon the body velocity and fluid velocity, which in turn was influenced by the displacement in the wave direction. To overcome this, displacements and velocities were estimated based upon previously calculated values. These values were only used in the determination of the sign change in the forcing function and were later recalculated.

Inputs to the computer program were chosen to simulate conditions relative to the Hibernia field. The latitude was specified at 47°N, wind speed 12 m/s and wind/wave direction 225° (south-east). Inertial and drag coefficients were each varied from 0.5 to 1.5 [British Ship Research Association (1976)] and the bergy-bit mass from 2000 tonnes to 10,000 tonnes. Wave heights were varied from 10 m to 20 m and wave periods from 11.0 secs to 13.8 secs.

RESULTS AND DISCUSSION

Verification of Computer Program

To ensure that the program was correct, the inputs were set so that there were no wind, current or Coriolis forces. The bergy-bit was given an initial velocity of -1.0 m/sec and after every 165.0 secs the iterative solution produced alternating negative and positive body displacements as shown in Table II. From this it was concluded that if the only forces acting on the bergy-bit are those due to wave motion, the bergy-bit will be only oscillating back and forth with a large period.

Review of Body and Fluid Acceleration

In all the subsequent discussions, the bergy-bit motion is influenced by the presence of wave, wind/wave current and Coriolis forces. Previously, when only wave excitation was considered, the averaged fluid velocity U_G reached a steady state in which the positive and negative portions of the cyclic motion were almost of the same magnitude for each wave period as shown in Table II. When wind/wave current effects were included, this added a component, which was not time dependent, to the fluid velocity (U_G); but the fluid acceleration ($\dot{U}_G$) which is the fluid velocity derivative, was not affected by the constant current components. Fig. 5 gives the acceleration components (southerly direction) of 2000t bergy-bit and the wave particle acceleration (H=10.0 m, T=11.0 secs). The body accelerations for 2000t, 5000t and 10,000t mass bergy-bits are in phase with the fluid accelerations but are lower (59.0%, 53.5%, 56.1% of maximum averaged fluid acceleration, respectively) due to the viscous damping.

Effect of Mass on Body and Fluid Accelerations

The magnitude of the peak fluid accelerations decreases slightly with increases in bergy-bit mass. The peak acceleration in Fig. 5 (mass = 2000 tons) is ± 0.95 m/s^2 (59% of maximum averaged fluid acceleration) compared to a peak acceleration of ± 0.83 m/s^2 (56.1% of maximum averaged fluid acceleration) for a mass of 10,000 t.

The change in the forcing function, which becomes increasingly significant with higher masses, causes a direct change in the system's viscous damping coefficient (C_1).

TABLE II BERGY-BIT MOTION DUE TO WAVE EXCITATION

Mass = 2000 t Wave Ht= 10.0 m Wave Period = 11s
$C_m = C_d = 1.5$

Time	Bergy-Bit			Fluid	
	Displacement	Velocity	Acceleration	Velocity	Acceleration
100.0	15.351	-1.250	-0.452	-1.760	-0.745
101.3	13.561	-1.552	-0.021	-2.300	-0.023
102.4	11.742	-1.286	0.433	-1.799	0.721
105.0	10.382	0.282	0.650	0.971	1.048
107.5	12.525	1.164	-0.024	2.295	-0.083
110.0	14.552	0.208	-0.651	0.739	-1.095
112.5	13.047	-1.318	-0.411	-1.868	-0.675
225.0	-10.361	-1.564	0.108	-2.270	0.187
227.5	-13.071	-0.371	0.670	-0.091	1.155
230.0	-12.046	1.021	0.277	2.156	0.404
231.3	-10.673	1.111	-0.134	2.240	-0.263
232.5	-9.500	0.710	-0.494	1.583	-0.839
235.0	-9.637	-0.867	-0.615	-1.043	-1.031
237.5	-13.040	-1.542	0.171	-2.227	0.289

For a mass of 2000 tons, the viscous damping coefficient in the southern direction was 84,572.09 N.sec/m (vide Table III) compared with a viscous damping of 1,870,804.2 N.sec/m for a mass of 10,000 tons, (with C_m&C_d = 1.5); whereas the corresponding maximum total forces were 2.86×10^6 N and 12.33×10^6 N, respectively.

TABLE III

Effect of Wave Height and Period on Damping Coefficient and Bergy-bit Velocity
(with wind, current, wave and coriolis effects)

Mass (t)	Wave height (m)	Period (Secs)	Damping Coefficient (N. sec/m)	U_G Max. Fluid Vel. (m. sec)	Body Vel. (% of U_G) (m/sec)
2,000	10	11	84,572.1	2.27	1.45 (64%)
	15	12.5	12,511.7	3.08	2.25 (73%)
	20	13.8	15,905.8	3.73	2.68 (72%)
5,000 t	10	11	433,025.5	2.18	1.13 (52%)
	15	12.5	281,948.6	2.97	1.75 (59%)
	20	13.8	61,601.1	3.63	2.50 (69%)
10,000 t	10	11.0	1,870,804.2	2.12	0.97 (46%)
	15	12.5	159,609.7	2.85	2.00 (70%)
	20	13.8	199,302.6	3.49	2.41 (69%)

This change in the viscous damping coefficient directly affects the interaction between fluid and body accelerations. In Fig. 5 the body has a mass of 2000t and the lowest viscous damping forces; its peak body acceleration is 59.0% of the fluid acceleration. In contrast, for Fig. 7, which has a body mass of 10,000 tons and the highest viscous damping forces, has a smaller peak body acceleration of 56.1% of the corresponding fluid

acceleration.

Review of Body and Fluid Velocities

When subjected only to wave excitation, the fluid particle velocities (U_G) follow a symmetric path without a net forward velocity component. Fig. 8 demonstrates the change in the velocity distribution when a net current resultant of -0.6634 m/sec is added in the southern direction. As seen in Fig. 8, the symmetrical nature of the fluid velocity distribution is affected, being lowered by the superposition of the current velocity component of -0.6634 m/sec in the -ve direction.

Effect of Mass on Body and Fluid Velocities

Although the average fluid particle (U_G) velocities are mostly affected by a change in wave/wind current components, they are also influenced by a change in bergy-bit mass, due to change in length of body. Table III shows that the average (over the body length) fluid velocities increase slightly with a decrease in body mass, due to a decrease in body length.

Review of Body Displacements

To obtain a better understanding of how bergy-bit displacements were affected by different conditions, the computer program was run for different masses with varying drag and inertial coefficients.

Effect of Varying Inertial Coefficients on Bergy-Bit Displacements

If the drag coefficient is held constant, the inertial force increases with increased inertial coefficients and increased mass. Figs. 9 and 10 correspond to the motion of the 2,000 t bergy-bit. These figures show relatively similar displacements for all three inertial coefficients. The smallest coefficient (C_m= 0.5) showed the greatest influence to current drift velocities which were largest in the southern direction (to the right of south east wind advance). The largest coefficient (C_m = 1.5) caused the least body displacements. The displacement given in Figs. 11 and 12 do not show a similar trend. The body drift velocity corresponding to C_m=0.5 was much greater than that for the remaining coefficients while the wind current drift was most noticeable for C_m=1.0 (due to the larger southward drift in Fig. 10). Figs. 13 and 14, corresponding to a mass of 10,000 tons, show a relationship similar to Fig. 9 & 10 representing a mass of 2,000 tons. Once again the smallest inertial coefficient showed the greatest influence on the bergy-bit motion and the largest inertial coefficient caused the least body displacement. One result which is obvious from Figs. 9 through 14 is that an increase in bergy-bit mass (and body dimensions) will cause a decrease in body velocity and thus body displacements. This is primarily due to the increased damping coefficients caused by an increase in the magnitude of the forcing function (Table III).

Effect of Varying Drag Coefficients on Bergy-Bit Displacements

Changes in the drag coefficients can make dramatic differences to body displacements and velocities. As previously mentioned, the inertial forces are in the order of 15 to 20 times larger than the drag forces and the system is inertially dominated. The effect of increasing drag coefficients is to increase the percentage of the drag force with respect to the total force. This reduces the inertial force effect upon the system. The drag force, whose sign is controlled by velocity conditions, is out of phase with the inertial force which depends on acceleration conditions. The two forces often have a negative effect when combined; therefore an increase in drag coefficients would tend to decrease the overall magnitude of the forcing function and result in low damping.

Following this reasoning, it is evident why the larger drag coefficients have the largest displacements and the smallest coefficients have the smallest displcements. This phenomenon can be seen in Figs. 15, 16, 19 and 20 representing masses of 2000 and 10,000

tons. However, for a mass of 5000 tons (Figs. 17 and 18) the smallest damping coefficient (C_1) is produced for a $C_d = 0.5$. When examining C_m coefficients it was suspected that this situation was drag dominated. This would give a possible explanation for the dramatic change in behavior in the overall magnitude and shape of the response function.

Wave Height and Wave Period Effects on Body Motion

Determining precise wave characteristics is a necessity when predicting bergy-bit motion. An increase in wave height and period leads to significant increases in both wave length and fluid velocities. For a mass of 2000 tons, increasing the wave height from 10 m to 20 m increases the wave length from 207.3 m to 311.3 m and the maximum fluid velocity from 2.27 m/s to 3.73 m/s respectively (for the wind current conditions previously studied). One of the reasons for the increase in fluid velocity was a substantial increase in the wave current component (from 0.396 m/s to 0.7238 m/s). Changing wave height and period also affects the forcing function and changes the damping of the system. These results indicate that the maximum body velocity is affected more by its damping compared to the body mass. They also show that smaller the damping, the closer the body velocity follows the fluid velocity and the larger the ratio $(\dot{X})$ bergy-bit/(U_G) of fluid particle.

CONCLUSIONS

The following conclusions were drawn from the studies reported and discussed in the earlier part of this report.

1. An increase in the mass of the system was found to correspond to an increased viscous damping forces which lead to reduced body velocities and net body displacements.

2. An increase in the drag coefficients was found to reduce the magnitude of the forcing function (due to a phase shift between the drag and inertial forces), and the viscous damping resulting in larger body velocities and displacements.

3. Exceptions to the general influence of inertial and drag coefficients on bergy-bit motion have occurred and have been attributed to a shift from an inertial to a drag dominated system (when the mass of the bergy-bit was 5,000 t).

5. The above procedure with a slight modification of input parameters would give the random motion of a bergy-bit under a storm wind condition (with varying wind directions).

6. For considering the rotational and translational motion of bergy-bits, the above equations are not sufficient; a coupled formulation becomes inevitable.

7. Overall bergy bit motion was governed by the extent to which the body velocities followed the fluid particle velocities. This was primarily determined by the viscous damping which was proportional to square of the body's excitation forces.

ACKNOWLEDGEMENTS

The authors would like to thank Dean Dr. G. R. Peters, and Prof. T. R. Chari, Associate Dean of the Faculty of Engineering and Applied Science, and Dr. I. Rusted, Vice President for their continued interest and encouragement. They would also like to express their sincere thanks to Dr. A. S. J. Swamidas, visiting Research Fellow, for his much appreciated assistance and his unfailing efforts during the course of this work. We thank Mr. H. El-Tahan for his interest and assistance in the completion of this study. The second author would like to gratefully acknowledge the funding provided by NSERC Undergraduate Research Award and Operating Grant A1779 and the support of Professor D. B. Muggeridge, Chairman, Ocean Engineering Research Group. We thank Mrs. Vatcher for the careful typing of the manuscript.

REFERENCES

British Ship Research Association, "A Critical Evaluation of Data on Wave Force Coefficients", OSFLAG Project 10, Report No. W278, 2 Volumes, 1976.

Craig Jr., R. R., Structural Dynamics: An Introduction to Computer Methods, John Wiley Sons, New York, 1981, pp. 146-151.

Dempster, R. T., "The Measurement and Modelling of Iceberg Drift", IEEE Conference on Oceans, Vol. 1, 1974.

Doyle, R., "Bergy-bit Motion Due to Wind, Wave Current and Coriolis Forces", Work Term Report submitted to Division of Coordination, Memorial University of Newfoundland, St. John's, Newfoundland, April, 1984, 83 pp.

El-Tahan, H., El-Tahan, M., and Venkatesh, S., "Forecast of Iceberg Ensemble Drift", Proceedings of Offshore Technology Conference, Houston, Texas, May 2-5, 1983, Paper No. OTC 4460, Vol. I, pp. 151-158.

Foldvik, A., Gammelsrod, T., and Gjessing, Y., "Measurements of Oscillations and Flexure of Icebergs", Annals of Glaciology, Vol. I, 1980, pp. 29-30.

Grande, N., and Guillaud, Ch., "Iceberg Stability and Draft Changes", Proceedings of III International Specialty Conference on Cold Regions Engineering on "Northern Resource Development", Edmonton, Alberta, April 4-6, 1984, Vol. I, pp. 459-471.

Goodman, D. J., Wadhams, P., and Squire, V.H., (1980) "The Flexural Response of a Tabular Ice Island to Ocean Swell", Annals of Glaciology, Vol. I, 1980, pp. 23-27.

Hooft, J.P., Advanced Dynamics of Marine Structures, John Wiley & Sons, New York, 1982, pp. 121-123.

Hsiung, C.C., and Aboul-Azm, A. F., "Iceberg Drift Affected by Wave Action", Ocean Engineering, January, 1983, 13 pp.

Lever, J., Reimer, E., and Diemand, D., "A Model Study of the Wave-Induced Motion of Small Icebergs and Bergy Bits", Proceedings of IIIrd International Symposium on Offshore Mechanics and Arctic Engineering, ASME, New Orleans, February, 1984, 10 pp.

Loo, H. L., "Studies on Wave Forces and Semi-submersible Bergy-bit Collision", Work Term Report submitted to Division of Coordination, Memorial University of Newfoundland, St. John's, Newfoundland, August, 1983, 98 pp.

Marex: Iceberg Severity Forecast, Proprietary Report, 1977.

Memos, C. D., "Effect of a Structure on Currents Induced by Waves and Winds", Proceedings of the Permanent International Association of Navigation Congresses Bulletin, Vol. 3, No. 34, 1979, pp. 47-52.

Morison, J. R.., O'Brien, M. D., Johnson, J. W., and Schaaf, S. A., "The Force Exerted by Surface Waves on Piles", Petroleum Transactions, Vol. 189, TP 2846, 1950, pp. 149-154.

Mountain, D. G., "On Predicting Iceberg Drift", Cold Regions Science and Technology, Vol. I, 1980, pp. 273-282.

Murray, J. E., "The Drift, Deterioration and Distribution of Icebergs in tghe North Atlantic Ocean", Ice Seminar (CIM Special Volume 10) 1969, pp. 3-18.

Murray, J. J., Muggeridge, D. B., and Guy, G. B., "Response of Modelled Ice Masses to Regular Waves and Irregular Wave Groups", Proceedings of the IEEE Conference on OCEANS '83, San Francisco, September, 1983.

Napoleoni, J. G. P., "The Dynamics of Iceberg Drift", Thesis submitted in partial fulfilment for M. A. Sc. Degree, Dept. of Geophysics and Astronomy, University of British Columbia, Aug, 1979, 90 pp.

NORDCO: Iceberg Survey 1975, Proprietary Report 1975.

Petroleum Directorate, Government of Newfoundland and Labrador, St. John's, Proceedings of a Symposium on "Production and Transportation System for the Hibernia Discovery", [Ed. W. E. Russell and D. B. Muggeridge], February, 1981.

Schwerdtfeger, P., "Iceberg Oscillations and Ocean Waves", Annals of Glaciology, Vol. 1, 1980, pp. 63-65.

Sodhi, D. S., and El-Tahan, M., "Prediction of an iceberg Drift Trajectory During a Storm", Annals of Glaciology, Vol. I, 1980, 00. 77-82.

Wright, B., and Berenger, D., "Ice Conditions Affecting Offshore Hydrocarbon Production in the Labrador Sea", InterMaritec Conference, Hamburg, Germany, September 23-27, 1980, pp. 50-62.

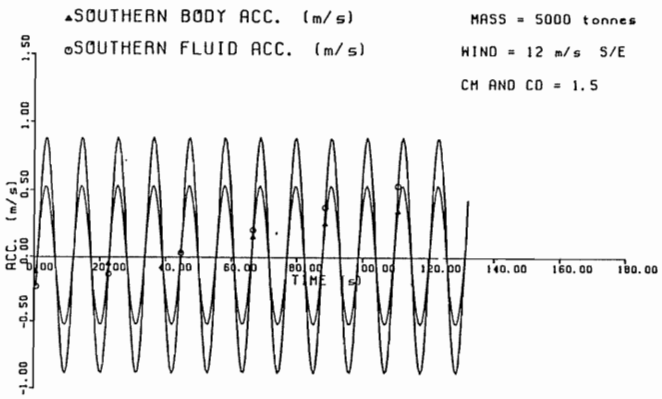

Fig. 5 Southerly acceleration component of the 2,000 t bergy-bit ($\ddot{X}$) and the wave ($\dot{u}_G$) as a function of time H = 10.0 m, T = 11.0 sec.

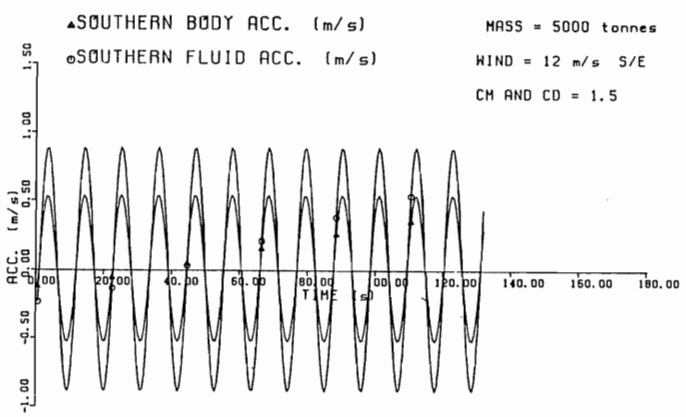

Fig. 6 Southerly acceleration component of the 5,000 t bergy-bit ($\ddot{X}$) and the wave ($\dot{u}_G$) as a function of time; H = 10.0 m, T = 11.0 secs.

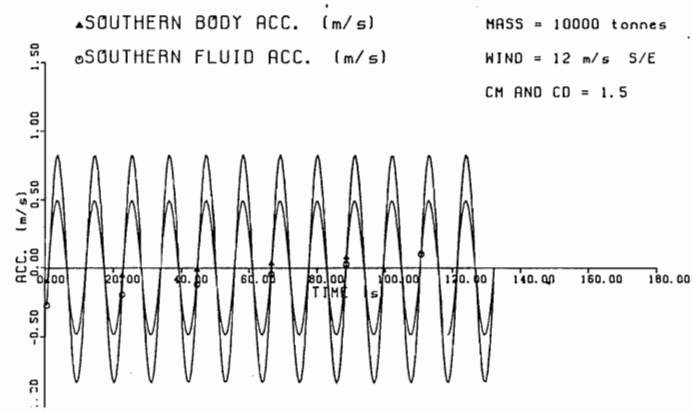

Fig. 7 Southerly acceleration component of the 10,000 t bergy-bit ($\ddot{X}$) and the wave ($\dot{u}_G$) as a function of time; H = 10.0, T = 11.0 secs.

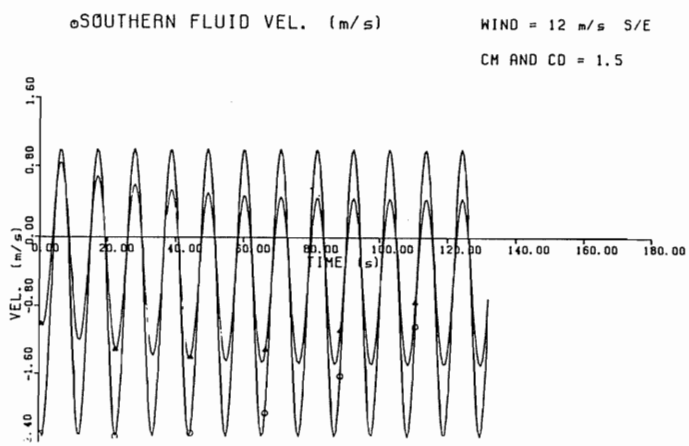

Fig. 8 Southerly velocity component of the 2,000 t bergy-bit ($\dot{X}$) and the wave (u_G) as a function of time for a wave of H = 10.0 m and T = 11.0 secs.

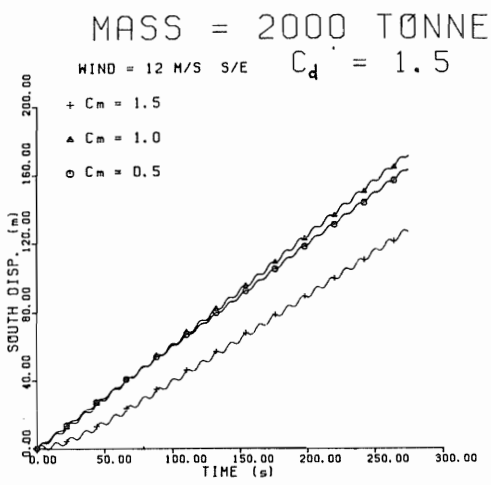

Fig. 9 Southerly motion of a 2,000 t bergy-bit as a function of time (H = 10.0 m; T = 11.0 secs)

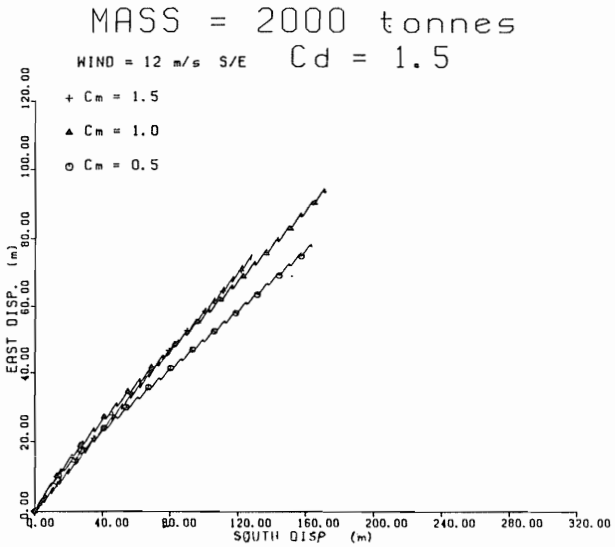

Fig. 10 Motion coordinates of a 2,000 t bergy-bit (H = 10.0 m; T = 11.0 secs)

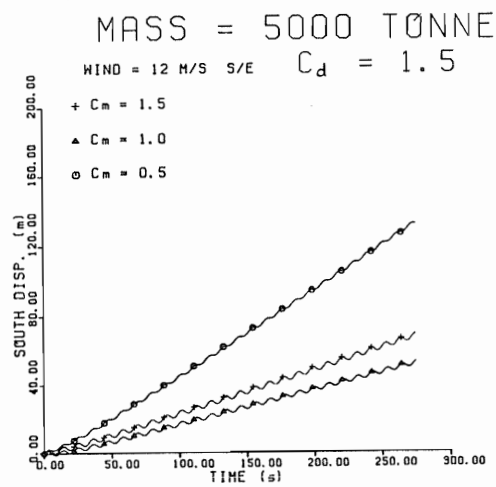

Fig. 11 Southerly motion of a 5,000 t bergy-bit as a function of time (H = 10.0 m; T = 11.0 secs)

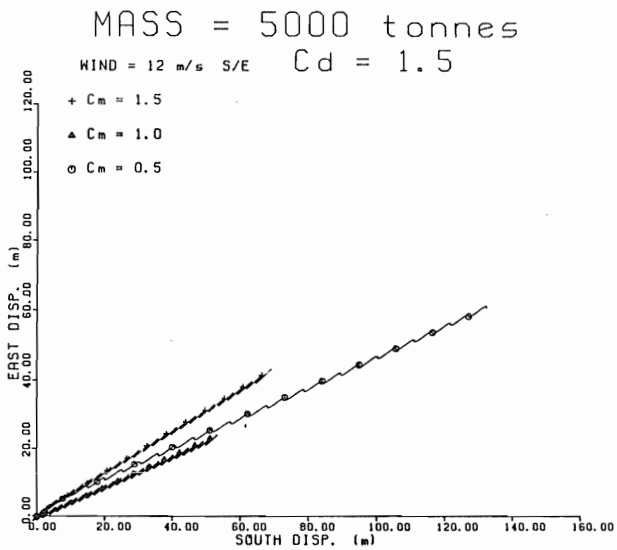

Fig. 12 Motion coordinates of a 5,000 t bergy-bit (H = 10.0 m; T = 11.0 secs)

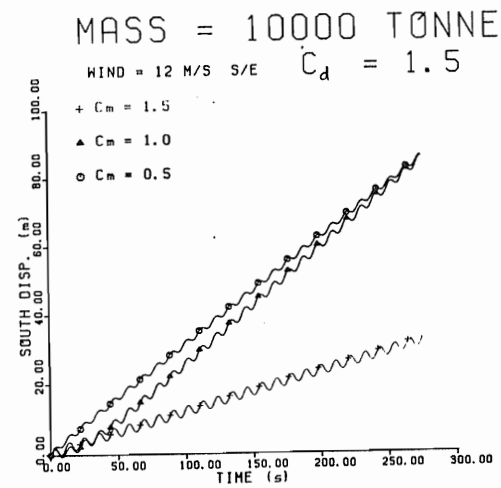

Fig. 13 Southerly motion of a 10,000 t bergy-bit as a function of time (H = 10.0 m; T = 11.0 secs)

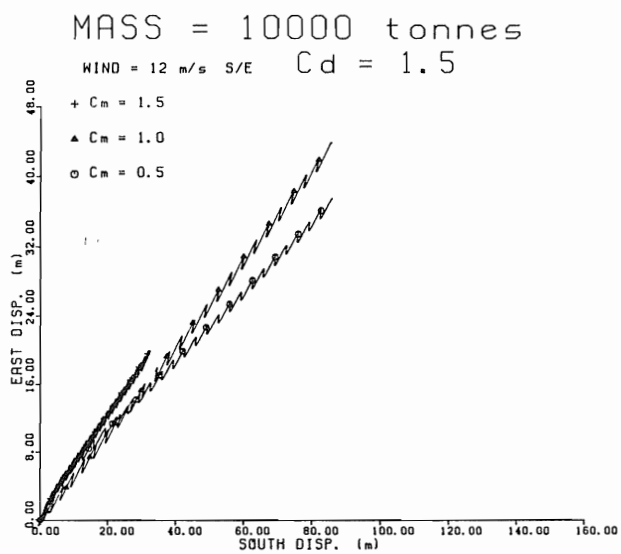

Fig. 14 Motion coordinates of a 10,000 t bergy-bit (H = 10.0 m; T = 11.0 secs)

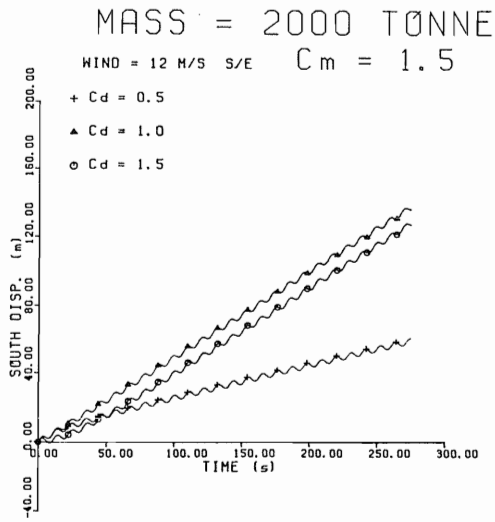

Fig. 15 Southerly motion of a 2,000 t bergy-bit as a function of time for varying drag coefficients (H = 10.0m; T = 11.0 secs).

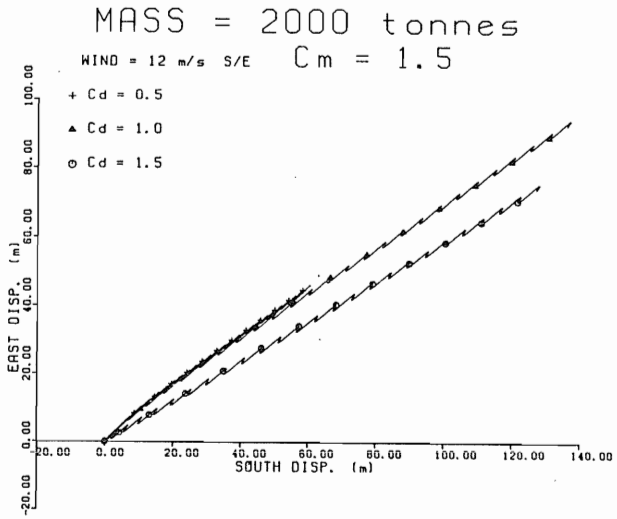

Fig. 16 Motion coordinates of a 2,000 t bergy-bit for varying drag coefficients (H = 10.0 m; T = 11.0 secs)

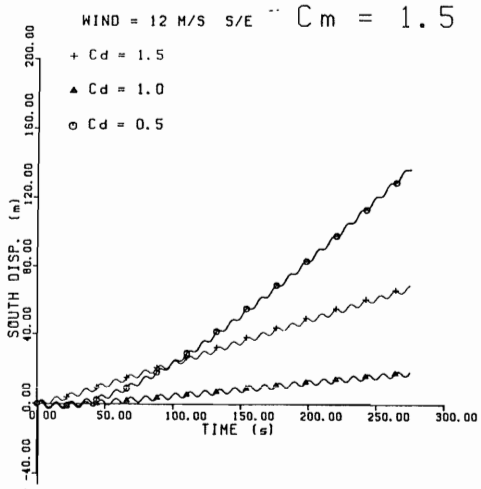

Fig. 17 Southerly motion of a 5,000 t bergy-bit as a function of time for varying drag coefficients (H = 10.0 m; T = 11.0 secs)

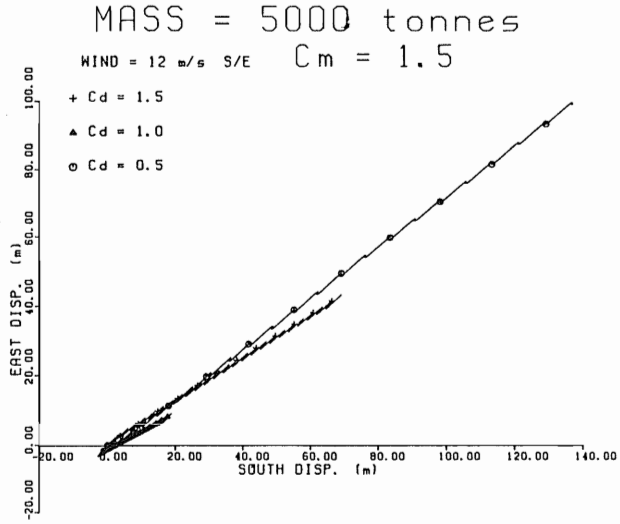

Fig. 18 Motion coordinates of a 5,000 t bergy-bit for varying drag coefficients (H = 10.0 m; T = 11.0 secs).

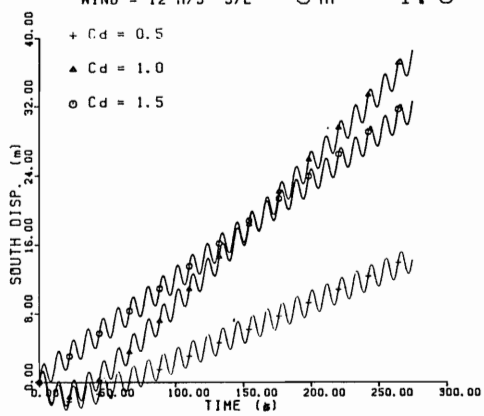

Fig. 19 Southerly motion of a 10,000 bergy-bit as a function of time for varying drag coefficients (H = 10.0 m; T = 11.0 secs).

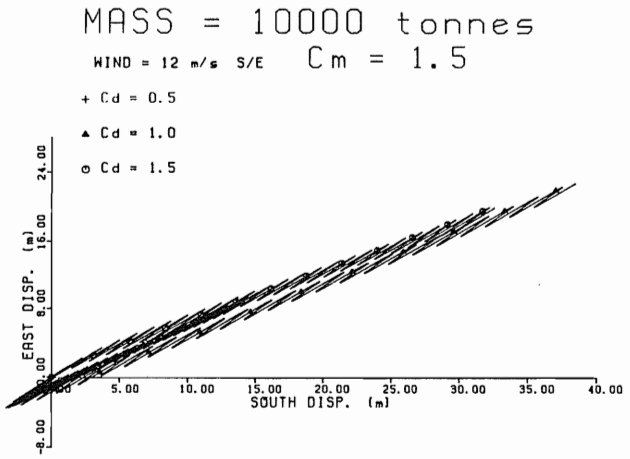

Fig. 20 Motion coordinates of a 10,000 t bergy-bit for varying drag coefficients (H = 10.0 m; T = 11.0 secs)